

SINDI: an Efficient Index for Approximate Maximum Inner Product Search on Sparse Vectors

Ruoxuan Li
ECNU, Shanghai, China
rxlee@stu.ecnu.edu.cn

Xiaoyao Zhong
Jiabao Jin
Ant Group, Shanghai, China
zhongxiaoyao.zxy@antgroup.com
jinjiabao.jjb@antgroup.com

Peng Cheng
Tongji University & ECNU
Shanghai, China
cspcheng@tongji.edu.cn

Wangze Ni
Zhejiang University
Hangzhou, China
niwangze@zju.edu.cn

Lei Chen
HKUST (GZ) & HKUST
Guangzhou & HK SAR, China
leichen@cse.ust.hk

Zhitao Shen
Ant Group, Shanghai, China
zhitao.szt@antgroup.com

Wei Jia
Xiangyu Wang
Ant Group, Shanghai, China
jw94525@antgroup.com
wxy407827@antgroup.com

Xuemin Lin
Shanghai Jiaotong University
Shanghai, China
xuemin.lin@gmail.com

Heng Tao Shen
Jingkuan Song
Tongji University, Shanghai, China
shenhengtao@hotmail.com
jingkuan.song@gmail.com

ABSTRACT

Sparse vector Maximum Inner Product Search (MIPS) is crucial in multi-path retrieval for Retrieval-Augmented Generation (RAG). Recent inverted index-based and graph-based algorithms have achieved high search accuracy with practical efficiency. However, their performance in production environments is often limited by redundant distance computations and frequent random memory accesses. Furthermore, the compressed storage format of sparse vectors hinders the use of SIMD acceleration. In this paper, we propose the *sparse inverted non-redundant distance index* (SINDI), which incorporates three key optimizations: (i) Efficient Inner Product Computation: SINDI leverages SIMD acceleration and eliminates redundant identifier lookups, enabling batched inner product computation; (ii) Memory-Friendly Design: SINDI replaces random memory accesses to original vectors with sequential accesses to inverted lists, substantially reducing memory-bound latency. (iii) Vector Pruning: SINDI retains only the high-magnitude non-zero entries of vectors, improving query throughput while maintaining accuracy. We evaluate SINDI on multiple real-world datasets. Experimental results show that SINDI achieves state-of-the-art performance across datasets of varying scales, languages, and models. On the MSMARCO dataset, when Recall@50 exceeds 99%, SINDI delivers single-thread query-per-second (QPS) improvements ranging from 4.2× to 26.4× compared with SEISMIC and PYANNS. Notably, SINDI has been integrated into Ant Group’s open-source vector search library, VSAG.

PVLDB Reference Format:

Ruoxuan Li, Xiaoyao Zhong, Jiabao Jin, Peng Cheng, Wangze Ni, Lei Chen, Zhitao Shen, Wei Jia, Xiangyu Wang, Xuemin Lin, Heng Tao Shen, and Jingkuan Song. SINDI: an Efficient Index for Approximate Maximum Inner Product Search on Sparse Vectors. PVLDB, 14(1): XXX-XXX, 2026. doi:XX.XX/XXX.XX

This work is licensed under the Creative Commons BY-NC-ND 4.0 International License. Visit <https://creativecommons.org/licenses/by-nc-nd/4.0/> to view a copy of this license. For any use beyond those covered by this license, obtain permission by

1 INTRODUCTION

Recently, retrieval-augmented generation (RAG) [7, 11, 12] become one of most successful information retrieval framework attracting attention from research communities and industry. Usually, texts are embedded into dense vectors (i.e., no dimension of the vector is zero entry) in RAG, then retrieved through approximate nearest neighbor search (ANNS) on their corresponding dense vectors.

To enhance the RAG framework, researchers find that using sparse vectors retrieval to complement dense vector based RAG can yield better overall accuracy and recall performance. Different from dense vectors, sparse vectors (i.e., only a very small portion of dimensions of sparse vectors are non-zero entries) are generated by specific models (e.g., SPLADE [4–6]) to preserve semantic information while enabling precise lexical matching [12]. In the enhanced RAG framework, dense vectors capture the holistic semantic similarity between texts and sparse vectors ensure exact term recall, therefore resulting in better overall performance. We show the process of the enhanced RAG in the following example:

Example 1. Precise lexical matching. *In the retriever stage of RAG, queries and documents are compared to select top-k candidates. Dense vectors capture semantic similarity, while sparse vectors support exact term matching. For example, “I love black cats” is tokenized into “i”, “love”, “black”, and “cats”, with “cats” assigned the highest weight (0.8). A query containing “cats” will precisely match documents where this token has a high weight. Challenges in inner-product computation. Dense vectors are stored contiguously, enabling parallel dot-product over consecutive dimensions via SIMD. Sparse vectors typically have very high dimensionality but store only their non-zero entries in a compact format, which*

emailing info@vldb.org. Copyright is held by the owner/author(s). Publication rights licensed to the VLDB Endowment.

Proceedings of the VLDB Endowment, Vol. 14, No. 1 ISSN 2150-8097. doi:XX.XX/XXX.XX

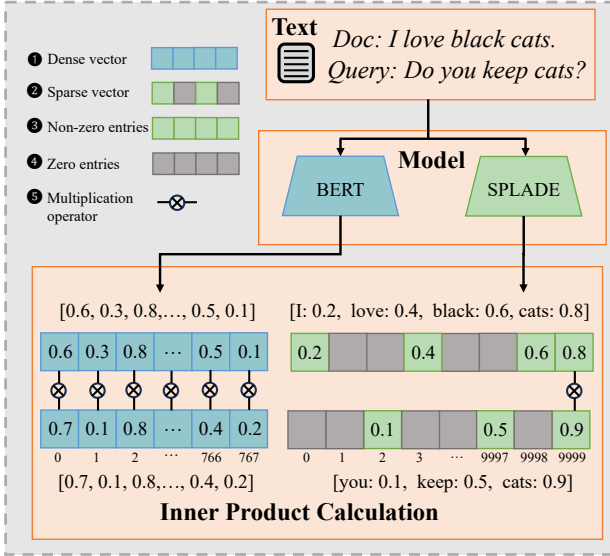


Figure 1: Example of Dense and Sparse Vector Representations and Inner Product Calculations.

leads to two bottlenecks: (1) ID lookup overhead: Matching common non-zero dimensions requires traversing all non-zero entries. Even if only one dimension (e.g., 9999) matches, all entries must be scanned. (2) No SIMD acceleration: Their storage is not dimension-aligned, preventing parallel SIMD processing.

The similarity retrieval problem for sparse vectors is formally known as the Maximum Inner Product Search (MIPS) [10, 15–17, 19], which aims to identify the top- k vectors in a dataset that have the largest inner product value with a given query vector. However, due to the curse of dimensionality [9], performing exact MIPS in high-dimensional spaces is computationally prohibitive. To mitigate this issue, we focus on Approximate Maximum Inner Product Search (AMIPS), which trades a small amount of recall for significantly improved search efficiency.

Many algorithms [2, 14, 18] have been proposed for AMIPS, employing techniques such as inverted index, proximity graphs, and hash-based partitioning. They improve efficiency by grouping similar vectors into the same partition, thereby reducing the number of candidates examined during query processing.

Despite reducing the search space, existing approaches still face two major performance bottlenecks: (i) *Distance computation cost*: Matching non-zero dimensions between a query and a document incurs substantial identifier lookup overhead, and the inner product computation cannot be effectively accelerated using SIMD instructions. (ii) *Random memory access cost*: During query processing, data are accessed in a random manner, and the variable lengths of sparse vectors further complicate direct access in memory.

To address the aforementioned challenges, we propose SINDI, a *Sparse Inverted Non-redundant Distance-calculation Index* for efficient sparse vector search. The main contributions of this paper are as follows: (i) *Value-Storing Inverted Index*: SINDI stores both vector

Table 1: Comparison to Existing Algorithms.

	SINDI(ours)	SEISMIC	PYANNS
Distance Complexity	$O\left(\frac{\ q\ }{s}\right)$	$O(\ q\ + \ x\)$	$O(\ q\ + \ x\)$
Memory Friendly	✓	✗	✗
SIMD Support	✓	✗	✗
QPS (Recall@50=99%)	241	58	24
Construction Time(s)	63	220	4163

identifiers and their corresponding values in the inverted index, enabling direct access during query processing; (ii) *Efficient Inner Product Computation*: SINDI eliminates redundant overhead in identifying common dimensions and fully exploits SIMD acceleration. By grouping values under the same dimension, SINDI enables batched inner product computation during queries; (iii) *Cache-Friendly Design*: SINDI reduces random memory accesses by avoiding fetches of original vectors. Instead, it sequentially accesses inverted lists for specific dimensions, thereby lowering cache miss rates. (iv) *Vector Mass Pruning*: SINDI retains only high-value non-zero entries in vectors, effectively reducing the search space and improving query throughput while preserving accuracy.

We compare SINDI with several state-of-the-art methods on the MSMARCO dataset (8.8M scale) in Table 1. The time complexity of computing the inner product between a query vector q and a document vector x using SINDI is $O\left(\frac{\|q\|}{s}\right)$, where the involved symbols are defined in Table 2. In contrast, inverted index and graph-based algorithms have a time complexity of $O(\|q\| + \|x\|)$. The detailed derivation is given in § 3.2.

In summary, the contributions of this paper are as follows:

- We present SINDI, a novel value-storing inverted index described in §3.1 and §3.2, which reduces redundant distance computation and random memory accesses. We further introduce a *Window Switch* strategy in §3.3 to support large-scale datasets.
- We propose *Vector Mass Pruning* in §4 to decrease the search space and improve query speed while maintaining accuracy.
- We evaluate SINDI on multi-scale, multilingual datasets in §5, demonstrating $4\times \sim 26\times$ higher single-thread QPS than PYANNS and SEISMIC at over 99% Recall@50, and achieving 8.8M-scale index construction in 60 seconds with minimal cost.

2 PRELIMINARIES

2.1 Problem Definition

Sparse vectors differ from dense vectors in that most of their dimensions have zero values. By storing only the non-zero entries, they significantly reduce storage and computation costs. We formalize the definition as follows.

Definition 1 (Sparse Vector and Non-zero Entries). *Let $\mathcal{D} \subseteq \mathbb{R}^d$ be a dataset of d -dimensional sparse vectors. For any $\vec{x} \in \mathcal{D}$, let x denote its sparse representation, defined as the set of non-zero entries:*

$$x = \{x^j \mid x^j \neq 0, j \in [0, d-1]\}.$$

Here, x^j denotes the value of \vec{x} in dimension j . The notation $\|x\|$ denotes the number of non-zero entries in x .

Table 2: Summary of Symbols

Symbol	Description
\mathcal{D}	base dataset
d	dimension of \mathcal{D}
\vec{x}, \vec{q}	base vector, query vector
$x, \ x\ $	sparse format of \vec{x} ; number of non-zero entries in x
\vec{x}_i, x_i	i -th base vector and its sparse format
x_i^j	value of \vec{x}_i in dimension j
s	SIMD width (elements per SIMD operation)
λ	window size
σ	number of windows
α	base vector pruning ratio
β	query vector pruning ratio
γ	reorder pool size
I, I_j	inverted index; inverted list for dimension j
$I_{j,w}$	w -th window of inverted list I_j
$T^j, T^j[t]$	temporary product array on dimension j ; value at index t
$A, A[m]$	distance array; value at index m
$\Omega(\vec{x}_1, \vec{x}_2)$	set of common non-zero dimensions of \vec{x}_1 and \vec{x}_2
$\delta(\vec{x}_1, \vec{x}_2)$	inner product of \vec{x}_1 and \vec{x}_2

To avoid confusion, we illustrate sparse vectors with an example in Figure 1.

Example 2. Consider the document “I love black cats” encoded into a sparse embedding: $[I : 0.2, \text{love} : 0.4, \text{black} : 0.6, \text{cats} : 0.8]$. The corresponding sparse representation is $x = \{x^0 = 0.2, x^3 = 0.4, x^{9998} = 0.6, x^{9999} = 0.8\}$, where $\|x\| = 4$.

Since the similarity measure in this work is based on the inner product, we formally define its computation on sparse vectors as follows.

Definition 2 (Inner Product on Sparse Vectors). Let $\vec{x}_1, \vec{x}_2 \in \mathcal{D}$, and let x_1 and x_2 denote their sparse representations. Define the set of common non-zero dimensions as

$$\Omega(\vec{x}_1, \vec{x}_2) = \{j \mid x_1^j \in x_1 \wedge x_2^j \in x_2\}.$$

The inner product between \vec{x}_1 and \vec{x}_2 is then given by

$$\delta(\vec{x}_1, \vec{x}_2) = \sum_{j \in \Omega(\vec{x}_1, \vec{x}_2)} x_1^j \cdot x_2^j.$$

Given the formal definition of the inner product for sparse vectors, we now define the Sparse Maximum Inner Product Search (Sparse-MIPS) task, which aims to find the vector in the dataset that maximizes this similarity measure with the query.

Definition 3 (Sparse Maximum Inner Product Search). Given a sparse dataset $\mathcal{D} \subseteq \mathbb{R}^d$ and a query point $\vec{q} \in \mathbb{R}^d$, the Sparse Maximum Inner Product Search (Sparse-MIPS) returns a vector $\vec{x}^* \in \mathcal{D}$ that has the maximum inner product with \vec{q} , i.e.,

$$\vec{x}^* = \arg \max_{\vec{x} \in \mathcal{D}} \delta(\vec{x}, \vec{q}). \quad (1)$$

For small datasets, exact Sparse-MIPS can be obtained by scanning all vectors. For large-scale high-dimensional collections, this is prohibitively expensive, and Approximate MIPS mitigates the cost by trading a small loss in accuracy for much higher efficiency.

Definition 4 (Approximate Sparse Maximum Inner Product Search). Given a sparse dataset $\mathcal{D} \subseteq \mathbb{R}^d$, a query point \vec{q} , and an approximation ratio $c \in (0, 1]$, let $\vec{x}^* \in \mathcal{D}$ be the vector that has the maximum

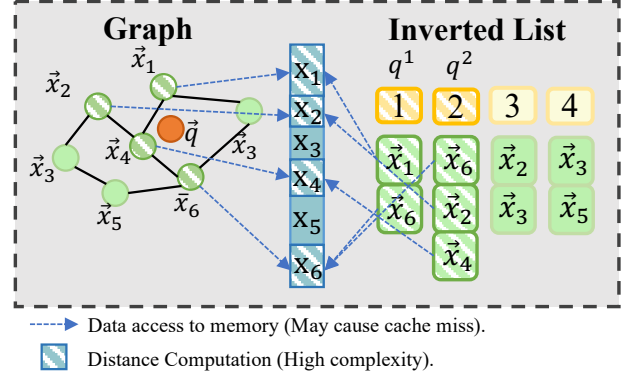


Figure 2: The bottleneck of the graph index and inverted index during searching process.

inner product with \vec{q} . A c -maximum inner product search (c -MIPS) returns a point $\vec{x} \in \mathcal{D}$ satisfying $\delta(\vec{q}, \vec{x}) \geq c \cdot \delta(\vec{q}, \vec{x}^*)$.

In practice, c -Sparse-MIPS methods can reduce query latency by orders of magnitude compared with exact search, making them preferable for large-scale, real-time applications such as web search, recommender systems, and computational advertising.

For ease of reference, the main notations and their meanings are summarized in Table 2, which will be referred to throughout the rest of the paper.

2.2 Existing Solutions

Representative algorithms for the AMIPS problem on sparse vectors include the inverted-index based SEISMIC [2], the graph based PYANNS. SEISMIC constructs an inverted list based on vector dimensions. PYANNS creates a proximity graph where similar vectors are connected as neighbors.

Example 3. Figure 2 illustrates a proximity graph and an inverted index constructed for \vec{x}_1 to \vec{x}_6 . Consider a query vector \vec{q} with two non-zero entries q^1 and q^2 . In the proximity graph, when the search reaches \vec{x}_4 , the algorithm computes distances between \vec{q} and all its neighbors, sequentially accessing x_1, x_2, x_4 , and x_6 from memory. In the inverted index, the algorithm traverses the posting lists for dimensions 1 and 2, accessing x_1, x_6, x_2 , and x_4 . Since vector access during search is essentially random, this incurs substantial random memory access overhead. Moreover, because $\|x\|$ varies across vectors, the distance computation between \vec{q} and \vec{x} has a time complexity of $O(\|q\| + \|x\|)$

Redundant Distance Computations. Sparse vectors incur high distance computation cost due to (i) the explicit lookup needed to identify the common dimensions $\Omega(\vec{x}, \vec{q})$ between a document \vec{x} and a query \vec{q} , resulting in complexity $O(\|q\| + \|x\|)$, and (ii) the inability of existing algorithms to exploit SIMD acceleration for inner product computation. Profiling 6980 queries on the MSMARCO dataset (1M vectors) using PERF and VTUNE shows that PYANNS spent 83.3% of CPU cycles on distance calculation.

Random Memory Accesses. The inefficiency of memory access in existing algorithms can be attributed to two main factors. First, they organize similar data points into the same partition and. To improve accuracy, vectors are replicated across multiple partitions.

This replication breaks the alignment between storage layout and query traversal order, preventing cache-friendly sequential access. During retrieval, the index returns candidate vector IDs, which incur random memory accesses to fetch their corresponding data, leading to frequent cache misses. Moreover, $\|x\|$ varies across sparse vectors, requiring offset table lookups to locate each vector’s data. In our measurements, SEISMIC averaged 5168 random vector accesses per query (5.1 MB), with an L3 cache miss rate of 67.68%.

3 FULL PRECISION INVERTED INDEX

This section introduces full-precision SINDI, an inverted index designed for sparse vector retrieval. Its advantages are organized along three aspects: index structure, distance computation, and cache optimization.

- In § 3.1 SINDI constructs a value-based inverted index by storing both vector identifiers and their corresponding dimension values in posting lists. This design eliminates the redundant dimension-matching overhead present in traditional inverted indexes.
- In § 3.2, SINDI employs a two-phase search process involving *product computation* and *accumulation*. By using SIMD instructions in multiplication, it reduces query complexity from $O(\|q\| + \|x\|)$ to $O\left(\frac{\|q\|}{s}\right)$. This maximizes CPU utilization and improves query throughput.
- In § 3.3, to mitigate cache misses caused by random access to the distance array, SINDI introduces *Window Switch* strategy, which partitions each posting list into fixed-size segments of length λ while using a shared distance array. This reduces memory overhead without increasing computation, and both theoretical analysis and experimental evaluation (Figure 5) demonstrate the existence of an optimal λ that minimizes memory access overhead.

3.1 Value-storing Inverted Index

Redundant inner product computations arise because identifying the common non-zero dimensions $\Omega(\vec{q}, \vec{x})$ between a query vector \vec{q} and a document vector \vec{x} requires scanning many irrelevant entries outside their intersection. We observe that the document identifiers retrieved from traversing an inverted list correspond precisely to the dimensions in $\Omega(\vec{x}, \vec{q})$. Therefore, when accessing a document \vec{x} from the list of dimension j , we can simultaneously retrieve its value x^j , thereby enabling direct computation of the inner product without incurring the overhead of finding $\Omega(\vec{q}, \vec{x})$.

Example 4. Figure 3 shows the inverted lists constructed for vectors x_1 to x_5 , comprising five term lists. When a query q arrives, it sequentially probes the inverted lists for dimensions 1, 3, and 5. The right side illustrates the common non-zero dimensions found when computing the inner product between the query and the documents. For example, in dimension 1, the inverted list retrieves x_2 and x_4 , and the inner-product computation also multiplies q with x_2^1 and x_4^1 . Therefore, the document IDs retrieved from the inverted lists overlap exactly with those used in finding common non-zero dimensions for the inner product. This indicates that we can compute the products of these non-zero entries during document retrieval itself.

Inspired by this observation, we extend the inverted list to store not only the ID i of each vector \vec{x}_i , but also its value x^j for the corresponding dimension j . This design eliminates the cost of searching

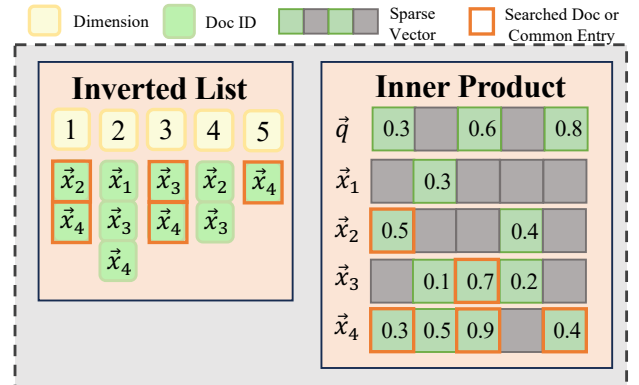


Figure 3: Overlap of Inverted List Entries and Common Non-Zero Dimensions in Inner-Product Computation.

$\Omega(\vec{x}_i, \vec{q})$ during the inner product computation, as well as the random memory access overhead for retrieving x_i .

3.2 Efficient Distance Computation

The entire query process of SINDI can be summarized into two stages: (1) *Product Computation*. Given an incoming query vector \vec{q} , for each non-zero q^j we fetch the j -th inverted list I_j , compute the products $q^j \times x_i^j$ for all $x_i^j \in I_j$, and temporarily store the results into the array T^j . (2) *Accumulation*. The values in T^j are accumulated into the distance array A . The length of A is set to $\|\mathcal{D}\|$, so that each entry $A[t]$ corresponds uniquely to a vector $\vec{x}_t \in \mathcal{D}$, allowing the accumulation from T^j to A to be completed in $\mathcal{O}(1)$ time per element. After completing the accumulation for all T^j with $q^j \in q$, each $A[t]$ contains $A[t] = \delta(\vec{x}_t, \vec{q})$. If $A[t] = 0$, it means that $\Omega(\vec{x}_t, \vec{q}) = \emptyset$.

Example 5. Figure 4 illustrates a query example. Since $\|\mathcal{D}\| = 9$, the distance array A is initialized with $\text{size}(A) = 9$ and all elements set to 0. The query \vec{q} contains three non-zero components q^1 , q^5 , and q^8 , thus only the inverted lists I_1 , I_5 , and I_8 need to be traversed. Take \vec{x}_4 as an example: in I_1 , the value is $x_4^1 = 6.8$, and the product with q^1 is 17.0, which is temporarily stored in $T[0]$. Accumulating to $A[4]$ gives $A[4] = 0 + 17.0 = 17.0$. Similarly, in I_5 we have $x_4^5 \times q^5 = 14.0$, which is stored in $T[2]$; adding $T[2]$ to $A[4]$ yields $A[4] = 31.0$. The computation for I_8 is analogous. Finally, we obtain $A[4] = 36.1$, which equals $\delta(\vec{x}_4, \vec{q})$. Although \vec{x}_4 has another non-zero entry x_4^2 , it does not contribute to the inner product and thus can be ignored. The same accumulation procedure applies to $\vec{x}_2, \vec{x}_3, \vec{x}_6$, and \vec{x}_7 . Eventually, $A[4]$ has the highest value, so the nearest neighbor of \vec{q} is \vec{x}_4 .

Using SIMD instructions, SINDI batch-processes the j -th inverted list I_j , multiplying q^j with each x_i^j it contains and writing the results sequentially into T^j . This not only utilizes CPU resources efficiently, but also reduces the time complexity of the inner product computation from $\mathcal{O}(\|v\| + \|q\|)$ to $\mathcal{O}\left(\frac{\|q\|}{s}\right)$, where s is the number of elements processed per SIMD operation. The derivation of the distance computation complexity for SINDI is as follows:

Theorem 3.1 (Amortized Time Complexity of SINDI Distance Computation). Let \mathcal{D} be the dataset, and let I denote an inverted

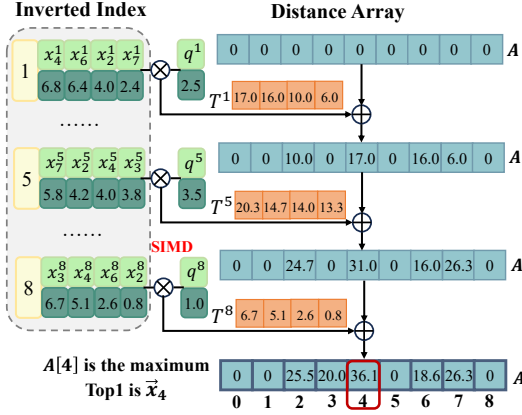


Figure 4: An example of SINDI index and query process.

index, and I_j is the j -th inverted list, let the set $\mathcal{I}^j = \{x_i^j \mid x_i^j \in x_i\}$ contains the non-zero entries in I_j .

Given a query vector \vec{q} , let $\mathcal{J} = \{j \mid q^j \in \vec{q}\}$ denote the set of dimensions containing non-zero entries in \vec{q} . Let $\mathcal{X} = \{\vec{x}_i \mid x_i^j \in x_i, j \in \mathcal{J}\}$ be the set of candidate vectors retrieved by \vec{q} .

Let s be the number of dimensions that can be processed simultaneously using SIMD instructions. Then, the per-vector time complexity of computing the inner product between \vec{q} and all $\vec{x}_i \in \mathcal{X}$ is

$$\Theta\left(\frac{\|\vec{q}\|}{s}\right).$$

Proof. The total number of non-zero entries accessed across all inverted lists corresponding to \mathcal{J} is:

$$\sum_{j \in \mathcal{J}} \|\mathcal{I}^j\|.$$

Since s dimensions can be processed in parallel using SIMD, the total time complexity for computing inner products between \vec{q} and all $\vec{x}_i \in \mathcal{X}$ is:

$$T_{\text{total}} = \sum_{j \in \mathcal{J}} \frac{\|\mathcal{I}^j\|}{s}.$$

The amortized complexity per vector is obtained by dividing T_{total} by the number of candidates $\|\mathcal{X}\|$:

$$T = \frac{T_{\text{total}}}{\|\mathcal{X}\|} = \frac{\sum_{j \in \mathcal{J}} \|\mathcal{I}^j\|}{s \cdot \|\mathcal{X}\|}.$$

In general, for any $\vec{x}_i \in \mathcal{X}$, we have $q \cap x_i \subseteq q$, implying that $\Omega(= \vec{x}_i, \vec{q})$ is at most $\|\vec{q}\|$. Therefore:

$$\sum_{j \in \mathcal{J}} \|\mathcal{I}^j\| \leq \sum_{\vec{x}_i \in \mathcal{X}} \|\vec{q}\|.$$

Substituting this relation into the expression for T yields:

$$T \leq \frac{\sum_{\vec{x}_i \in \mathcal{X}} \|\vec{q}\|}{s \cdot \|\mathcal{X}\|} = \frac{\|\vec{q}\| \cdot \|\mathcal{X}\|}{s \cdot \|\mathcal{X}\|} = \frac{\|\vec{q}\|}{s}.$$

Hence, the per-vector time complexity is:

$$\Theta\left(\frac{\|\vec{q}\|}{s}\right).$$

□

Algorithm 1: PreciseSINDIConstruction

Input: A sparse dataset \mathcal{D} and dimension d , window size λ

Output: Inverted list I

```

1 for  $j \in \{0, \dots, d-1\}$  do
2    $\mathcal{X} \leftarrow \{\vec{x}_i \mid x_i^j \in x_i, \vec{x}_i \in \mathcal{D}\}$ ;
3   foreach  $\vec{x}_i \in \mathcal{X}$  do
4      $w \leftarrow \lfloor \frac{i}{\lambda} \rfloor$ 
5      $I_{j,w}.append(x_i^j)$ 
6 return  $I$ 

```

In summary, the SINDI index eliminates the overhead of redundant term searches and enables SIMD to compute inner products in batches, fully leveraging the CPU's computational power. Moreover, it avoids the memory access costs associated with traversing the original vectors. Instead, the required values can be directly retrieved from the lists, allowing in-place product computation.

3.3 Cache Optimization

When the dataset size \mathcal{D} reaches the million scale, the distance array becomes very large. Random access to such a long array leads to frequent cache misses, causing the query performance to be highly memory-bound. Moreover, maintaining a distance array of size \mathcal{D} for every query consumes significant memory resources. To limit the length of the distance array, SINDI employs the *Window Switch* strategy that restricts the range of vector IDs accessed in a single window. Within each window, the reduced size of the distance array makes the access pattern nearly sequential.

3.3.1 Window Switch. During index construction, SINDI partitions the dataset \mathcal{D} into contiguous ID segments, referred to as windows. The window size is denoted by λ ($0 < \lambda \leq \|\mathcal{D}\|$), and the total number of windows σ is $\lfloor \frac{\|\mathcal{D}\|}{\lambda} \rfloor$. The w -th window contains vectors from $\vec{x}_{w\lambda}$ to $\vec{x}_{(w+1)\lambda-1}$, and the window index to which vector \vec{x}_i belongs is $\lfloor \frac{i}{\lambda} \rfloor$. Each inverted list is partitioned in the same way, so every list has σ windows. We denote the w -th window of the j -th inverted list by $I_{j,w}$, with $0 \leq w < \sigma$.

At query time, the length of the distance array A is set to the window size λ , and all windows share the same A . During a window search, each vector \vec{x}_i is mapped to a unique entry $A[i \bmod \lambda]$. The search procedure in the w -th window consists of two steps: (1) **Inner product computation.** For each scanned list, compute inner products for vectors $\vec{x}_{w\lambda}$ to $\vec{x}_{(w+1)\lambda-1}$. The computation follows the same two-stage process as described in Section 3.2, namely, product computation followed by accumulation. (2) **Heap update.** After computing the inner product for the current window, the distance array A contains the final distance. Scan A to insert the top candidates (with the largest inner products) into a minimum heap H , which maintains the vector IDs and distances of the results to be returned. Note that we need to recover the vector ID from A 's index, $A[t]$ corresponds to $\vec{x}_{t+\lambda \times w}$.

Clearly, *Window Switch* changes only the order of list entries scanned and does not affect the total number of computations. Therefore, the time complexity of distance computation remains $\mathcal{O}\left(\frac{\|\vec{q}\|}{s}\right)$.

3.3.2 Construction and Search. The construction process of the full-precision SINDI index with *Window Switch* is detailed in Algorithm 1. Given a sparse vector dataset \mathcal{D} with maximum dimension d . For each dimension j (Line 1), all vectors \bar{x}_i in \mathcal{D} with x_i^j in x_i are collected into a temporary set \mathcal{X} (Line 2). These vectors are then appended into the corresponding windows of the inverted list j based on their IDs (Lines 3-5). Finally, the constructed index I is returned after processing all dimensions (Line 6). The time complexity of the construction process is $O(\|\mathcal{D}\|\|\bar{x}\|)$, where $\|\bar{x}\|$ represents the average number of non-zero entries, that is $\frac{\sum_{\bar{x}_i \in \mathcal{D}} \|\bar{x}_i\|}{\|\mathcal{D}\|}$.

The search process for the full-precision SINDI index is summarized in Algorithm 2, consisting of three main stages: product computation, accumulation, and heap update. Given a query \vec{q} , an inverted index I , and the recall number of nearest neighbors k , the algorithm initializes a distance array A with length equal to λ , setting all elements to zero (Lines 1–2), and creates an empty min-heap H (Line 3). The outer loop iterates over all windows $w \in \{0, \dots, \sigma - 1\}$ (Line 4). For each non-zero query component $q^j \in \vec{q}$ (Line 5), the algorithm performs SIMD-based batched multiplication between q^j and all components x_i^j contained in $I_{j,w}$, storing the results sequentially into the temporary product array T^j (Line 6). Next, it retrieves each x_i^j in $I_{j,w}$ (Lines 7-8), computes the mapped index m of A (Line 9), and accumulates $T^j[t]$ into $A[m]$ (Line 10). After processing all $q^j \in q$ for the current window, the algorithm proceeds to the heap update stage (Line 12). For each entry in A , if $A[m]$ is greater than the current minimum in H or if the heap contains fewer than k elements, the algorithm inserts the corresponding global vector ID ($m + \lambda \times w$) along with its distance $A[m]$ into the heap (Lines 13–14). If the heap exceeds size k , the smallest element is removed (Lines 15–16). Finally, $A[m]$ is reset to zero to prepare for the next window (Line 17). After all windows have been processed, the heap H contains at most k vector IDs paired with their full-precision distances to the query, which is returned as the final result (Line 20).

Complexity. Assuming l is the average of non-zero entries in the traversed list, that is $l = \frac{\sum_{q^j \in q} I_{j, \text{size}()} }{\|q\|}$. Even with *Window Switch*, the total number of non-zero entries traversed remains constant, which is $\|q\|l$. Therefore, the time complexity of a full-precision query is $O(\frac{\|q\|l}{s})$. In conclusion, the computational cost of querying is independent of λ .

3.4 Analysis of Window Size’s Impact on Performance

While the *Window Switch* strategy does not change the overall computational complexity, it has a significant impact on memory access costs. When λ decreases, the distance array becomes shorter, leading to a lower cache-miss rate during random writes. However, the number of windows $\sigma = \frac{\|\mathcal{D}\|}{\lambda}$ increases, causing more frequent random accesses when switching between inverted sub-lists. Therefore, an appropriate choice of λ is required to balance these two effects. The following example can illustrate this:

Example 6. Figure 5 reports experimental results for the full-precision SINDI on the SPLADE-1M and SPLADE-FULL datasets. For each dataset, we executed 6,980 queries under different window sizes λ and measured the QPS. In addition, we used the Intel VTune

Algorithm 2: PreciseSINDISearch

Input: Query \vec{q} , an inverted list I , and k
Output: At most k points in \mathcal{D}

```

1 for  $m \in \{0, \dots, \lambda - 1\}$  do
2    $A[m] \leftarrow 0$ 
3 Initialize  $H$  is an empty minimum heap;
4 for  $w \in \{0, \dots, \sigma - 1\}$  do
5   foreach  $q^j \in q$  do
6      $T^j \leftarrow \text{SIMDProduct}(q^j, I_{j,w})$ ;
7     for  $t \in \{0, \dots, I_{j,w}.\text{size}() - 1\}$  do
8        $x_i^j \leftarrow I_{j,w}[t]$ ;
9        $m \leftarrow i \bmod \lambda$ ;
10       $A[m] \leftarrow A[m] + T^j[t]$ ;
11   for  $m \in \{0, \dots, \lambda - 1\}$  do
12     if  $A[m] > H.\text{min}()$  or  $H.\text{len}() < k$  then
13        $H.\text{insert}(m + \lambda \times w, A[m])$ 
14     if  $H.\text{len}() = k + 1$  then
15        $H.\text{pop}()$ 
16      $A[m] \leftarrow 0$ 
17 return  $H$ 

```

Profiler to record memory bound metrics for two types of memory accesses: distance array updates and sub-list switches. Here, memory bound refers to the percentage of execution time stalled due to memory accesses. For the SPLADE-1M dataset, as λ increases from 1K to 1M, the distance array miss rate decreases monotonically, while the sub-list switching miss rate increases monotonically. The total memory-bound latency reaches its minimum near $\lambda \approx 100K$, corresponding to the highest query throughput. The SPLADE-FULL dataset exhibits the same trend, confirming the existence of an optimal window size.

Based on this, the memory access latency for queries can be expressed in a double power-law form [1, 8] as follows:

$$T_{\text{mem}}(\lambda) = A\lambda^{+\alpha} + B\lambda^{-\beta} + C, \quad (2)$$

where:

- The independent variable is the window size λ ;
- The term $A\lambda^{+\alpha}$ captures the increasing cost of distance array cache misses as λ grows;
- The term $B\lambda^{-\beta}$ reflects the decreasing cost of sub-list switching misses with larger λ ,
- The constant C represents baseline memory access costs unrelated to λ .

According to the properties of the double power-law function, $T_{\text{mem}}(\lambda)$ reaches its minimum at $\lambda^* = \left(\frac{B\beta}{A\alpha}\right)^{\frac{1}{\alpha+\beta}}$. For small $\lambda \ll \lambda^*$, T_{mem} is dominated by the sub-list switching term and decreases as λ grows. For large $\lambda \gg \lambda^*$, the distance-array term dominates and T_{mem} increases with λ . The optimum $\lambda = \lambda^*$ occurs when the two terms balance.

Example 7. Figure 5 shows that the dashed line represents the theoretical QPS curve. It’s derived by estimating (α, β) via log–log

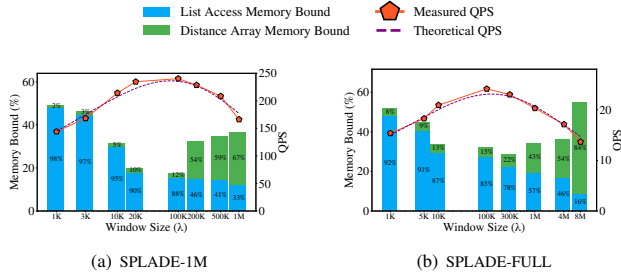


Figure 5: Impact of Window Size on Query Throughput and Memory Accesses.

regression and (A, B, C) via least-squares fitting of the double power-law model. For the SPLADE-1M dataset, the model predicts an optimal $\lambda^* \approx 7.35 \times 10^4$, while for SPLADE-FULL it predicts $\lambda^* \approx 1.25 \times 10^5$. These predictions are of the same order as the measured optimal $\lambda \approx 10^5$, with small deviations attributable to model abstraction and measurement variability. This agreement in both magnitude and trend supports the validity of our scaling analysis.

4 APPROXIMATE INVERTED INDEX

We focus on optimizing the query process through pruning and re-ranking. *Pruning* reduces the size of vectors or lists to improve search efficiency, while *re-ranking* compensates for pruning-induced precision loss by computing full inner products for a select set of candidates. Together, these techniques achieve a significant performance boost with only a minimal sacrifice in accuracy.

4.1 Pruning Strategies

A notable advantage of sparse vectors is that a small number of high-valued non-zero entries can represent most of the information in the entire vector [6]. This property arises from the training mechanisms of sparse models. For example, SPLADE tends to concentrate important information in a few non-zero dimensions. From a semantic perspective, many low-valued non-zero entries correspond to stopwords (e.g., “is”, “the”), which can be pruned.

Let \vec{x}'_i denote the pruned version of document \vec{x}_i , and \vec{q}' the pruned version of query \vec{q} , l is the average length of list before pruning, l' is the average length of list after pruning. The reduction in computational cost achieved by pruning is

$$\|q\|l - \|q'\|l'$$

while the *inner product error* ϵ introduced is

$$\epsilon = \sum_{\vec{x}_i \in \mathcal{D}} \left(\delta(\vec{x}_i, \vec{q}) - \delta(\vec{x}'_i, \vec{q}') \right).$$

Smaller $\|\vec{x}'_i\|$ leads to higher throughput gains, but also larger inner product error. Therefore, pruning must be designed with a trade-off between efficiency and accuracy. The following example shows that it is possible to retain only part of the non-zero entries while incurring only a small loss in inner product accuracy.

Example 8. We prune each document vector \vec{x}_i and the query vector \vec{q} by retaining only the non-zero entries with the largest absolute values, producing \vec{x}'_i and \vec{q}' . We vary the pruning ratio, defined

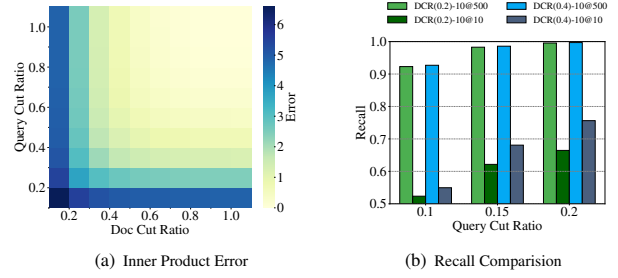


Figure 6: Intuition of Pruning and Reorder

as $\frac{\|\vec{x}'_i\|}{\|\vec{x}_i\|}$, to control the proportion of entries preserved. Figure 6(a) shows the corresponding inner product error under different pruning ratios. The results indicate that the error decreases sharply as the ratio increases from 0.1 to 0.3, and becomes nearly zero when the ratio is between 0.5 and 1, revealing a saturation effect of pruning ratio on inner product error.

As discussed in Section 3, for full-precision SINDI the upper bound for computing the inner product between \vec{x}_i and \vec{q} is $\Theta\left(\frac{\|q\|}{s}\right)$. For a given \vec{q} , the overall time complexity of the query process is $\mathcal{O}\left(\frac{\|q\|l}{s}\right)$, where l is the average number of inverted lists traversed. Reducing query latency therefore amounts to reducing l , $\|x\|$, and $\|q\|$. This can be approached from three directions: pruning lists, pruning documents, and pruning queries. List pruning and document pruning are applied during the index-construction stage, while query pruning is applied at query time. In this work, we mainly focus on the construction stage, as query pruning and document pruning are essentially both forms of vector pruning. We compare three pruning strategies—list pruning, document-count pruning, and quality-ratio pruning—and analyze their respective advantages and disadvantages:

List Pruning (LP). LP operates at the inverted-list level: for each dimension j , only the non-zero entries with the largest absolute values are retained in its inverted list I_j , restricting the list length to l' . Since the size of I_j varies across dimensions, highly valued $|x'_i|^j$ entries in longer lists may be pruned, while lower-valued non-zero entries in shorter lists are retained. After this list-wise pruning, each document vector \vec{x}_i is transformed into a pruned version $\phi_{LP}(\vec{x}_i)$ containing only those coordinates that survive the list truncation.

Vector Number Pruning (VNP). VNP reduces dimensionality at the vector level. Its core idea is to retain, for each vector \vec{x}_i , the vn non-zero entries with the largest magnitudes, so that $\|\vec{x}'_i\| = vn$. However, since $\|x_i\|$ varies across vectors, this scheme cannot consistently preserve the non-zero entries that contribute the most to the inner product computation.

Vector Number Pruning (VNP). VNP applies the pruning operator ϕ_{VNP} at the vector level. For each document vector \vec{x}_i , $\phi_{VNP}(\vec{x}_i)$ retains only the vn non-zero entries with the largest absolute values, so that $\|\phi_{VNP}(\vec{x}_i)\| = vn$. Since $\|\vec{x}_i\|$ varies across vectors, this scheme cannot consistently preserve the non-zero entries that contribute the most to the inner product computation.

Mass Ratio Pruning (MRP). MRP applies the pruning operator ϕ_{MRP} based on the cumulative sum of absolute values of a vector’s

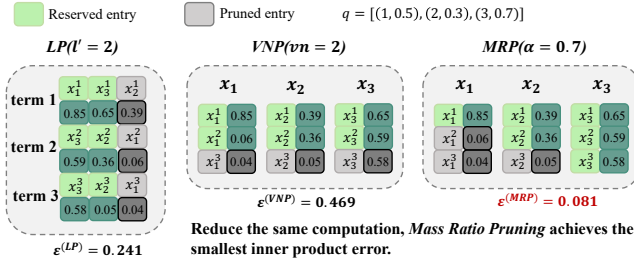


Figure 7: An example of List Pruning, Vector Number Pruning and Mass Ratio Pruning.

non-zero entries. For each document vector \vec{x}_i , $\phi_{\text{MRP}}(\vec{x}_i)$ ranks all non-zero entries in descending order of absolute value and retains the smallest prefix whose cumulative sum reaches a target fraction α of the vector’s total mass. This adaptive scheme discards low-value components that contribute little to the inner product while allowing vectors with different value-distribution to keep variable numbers of entries, reducing inverted list size without imposing a uniform length limit.

To formally introduce MRP, we first define the mass of a vector as the sum of the absolute values of its non-zero entries.

Definition 5 (Mass of a Vector). Let $\vec{x} \in \mathbb{R}^d$ be a vector. The mass of \vec{x} is defined as the sum of the absolute values of x ’s non-zero entries:

$$\xi(\vec{x}) = \sum_{x^j \in x} |x^j|.$$

Then we define the α -mass subvector as the shortest prefix of sorted non-zero entries whose cumulative absolute value reaches a fraction α of the total mass.

Definition 6 (α -Mass Subvector). Consider a vector $\vec{x} \in \mathbb{R}^d$ and a permutation π that orders the non-zero entries of \vec{x} by non-increasing absolute value, i.e. $|x^{\pi_j}| \geq |x^{\pi_{j+1}}|$. For a constant $\alpha \in (0, 1]$, let $1 \leq r \leq \|x\|$ be the smallest integer satisfying

$$\sum_{j=1}^r |x^{\pi_j}| \leq \alpha \xi(\vec{x}).$$

The collection $x'_{-\alpha} = \{x^{\pi_j}\}_{j=1}^r$ is the sparse representation of a vector $\vec{x}_{-\alpha}$, where $\vec{x}_{-\alpha}$ is the α -mass subvector of \vec{x} .

Example 9. Figure 7 illustrates three pruning methods applied to sparse vectors \vec{x}_1 , \vec{x}_2 , and \vec{x}_3 . List Pruning prunes each list to size $l' = 2$, Vector Number Pruning retains $vn = 2$ top entries of each vector, and Mass Ratio Pruning prunes each vector \vec{x}_i to $\vec{x}_{i,\alpha}$ with $\alpha = 0.7$. The pruning result is shown in the figure: (i) the three strategies all reduce the same computation, which is $\|q\|l - \|q'\|l' = 9 - 6 = 3$; (ii) Mass Ratio Pruning’s inner product error is the smallest. The reason is that List Pruning fails to retain the larger value x_2^1 , as each list is limited to a maximum of 2 vectors. Similarly, Vector Number Pruning does not retain x_3^3 . In contrast, Mass Ratio Pruning minimizes error by prioritizing influential entries.

Algorithm 3 outlines the process for constructing the approximate version of the SINDI index. Given a sparse vector dataset \mathcal{D} , maximum dimension d , window size λ , and pruning ratio α , the algorithm begins by initializing an empty set \mathcal{D}' to store pruned vectors (Line

Algorithm 3: APPROXIMATESINDICONSTRUCTION

Input: Sparse dataset \mathcal{D} of dimension d ; window size λ ; pruning ratio α

Output: Inverted index I

- 1 $\mathcal{D}' \leftarrow \emptyset$
 - 2 **foreach** $\vec{x}_i \in \mathcal{D}$ **do**
 - 3 $\vec{x}_{i-\alpha} \leftarrow \alpha$ -mass vector of \vec{x}_i
 - 4 $\mathcal{D}' \leftarrow \mathcal{D}' \cup \vec{x}_{i-\alpha}$
 - 5 $I = \text{PRECISESINDICONSTRUCTION}(\mathcal{D}', d, \lambda)$
 - 6 **return** I and \mathcal{D}
-

Algorithm 4: APPROXIMATESINDISEARCH

Input: Query \vec{q} , an inverted index I , query prune ratio β , reorder number γ , and k

Output: At most k points in \mathcal{D}

- 1 H is an empty *minimum heap*;
 - 2 R is an empty *minimum heap*;
 - 3 $\vec{q}_{-\alpha} \leftarrow \alpha$ -mass vector of \vec{q}
 - 4 $H = \text{PRECISESINDISEARCH}(\vec{q}_{-\alpha}, I, \gamma)$
 - 5 **while** $!H.empty()$ **do**
 - 6 $i, dis \leftarrow H.pop()$;
 - 7 $dis' \leftarrow \delta(\vec{x}_i, \vec{q})$;
 - 8 **if** $dis' > R.min()$ **or** $R.len() < k$ **then**
 - 9 $R.insert(i, dis')$
 - 10 **if** $R.len() = k + 1$ **then**
 - 11 $R.pop()$
 - 12 **return** R
-

1). For each vector x_i in \mathcal{D} (Line 2), its α -mass subvector is derived and assigned to $\vec{x}'_{i-\alpha}$ (Line 3). The remaining steps are identical to the full-precision index construction process, with the exception that the approximate index stores the original dataset to enable reordering during retrieval.

Figure 6(a) shows that retaining less than half of the non-zero entries in a query can reduce the inner product error to nearly zero. This significantly reduces the search space, shrinking it by more than half. It indicates that the term lists corresponding to a few high-value non-zero entries in the query already cover most recall points. Therefore, SINDI applies *Mass Vector Pruning* to queries as well.

4.2 Reordering

Retaining a small portion of non-zero entries can preserve most of the inner product but fails to maintain the partial order of the full inner product. Using pruned results directly for recall reduces accuracy. However, experiments show that with enough candidates, the nearest neighbors are likely to be included. Figure 6(b) shows Recall 10@500 and Recall 10@10 under different pruning ratios for documents and queries. Retaining 16% of document entries and 30% of query entries achieves Recall 10@500=0.98, but Recall 10@10 is only 0.63. This suggests a two-step strategy: first, perform coarse recall with the pruned index to retrieve many candidates, then refine them using full inner product reordering for efficient AMIPS.

Table 3: Dataset statistics and characteristics

Dataset	$\ \mathcal{D}\ $	$avg \ x_i\ $	nq	$avg \ q\ $	d	<i>Sparsity</i>	<i>Size (GB)</i>	<i>avg l</i>	<i>Model</i>	<i>Language</i>
SPLADE-1M	1,000,000	126.3	6980	49.1	30108	0.9958	0.94	4569.2	splade	English
SPLADE-FULL	8,841,823	126.8	6980	49.1	30108	0.9958	8.42	40447.3	splade	English
AntSparse-1M	1,000,000	40.1	1000	5.8	250000	0.9998	0.31	902.6	bge-m3	Chinese
AntSparse-10M	10,000,000	40.1	1000	5.8	250000	0.9998	3.06	6560.7	bge-m3	Chinese
NQ	2,681,468	149.4	3452	47.0	30510	0.9951	3.01	13914.7	splade	English
RANDOM-5M	5,000,000	150.0	5000	50.4	30000	0.9950	5.62	25000.0	-	-

Detail of Algorithm 4 Algorithm 4 details the query procedure for the approximate SINDI index. Given a query q , an inverted index I , query pruning ratio β , re-ranking threshold γ , and the number of nearest neighbors k , the algorithm starts by initializing two empty min-heaps, H and R , for storing coarse recall candidates and final top- k neighbors, respectively (Lines 1-2). The β ratio subvector q' of the query q is then generated (Line 3), and Algorithm 2 is invoked to retrieve γ coarse recall results into H (Line 4). While H is not empty (Line 5), the algorithm processes its top element by extracting the stored vector ID i and partial inner product score dis (Line 6). The full inner product between x_i and the original query q is calculated as dis' (Line 7). The tuple (i, dis') is inserted into heap R , maintaining its size at most k by removing the smallest element if necessary (Lines 8-11). This process continues until all coarse recall candidates in H are processed.

5 EXPERIMENTAL STUDY

5.1 Experimental Settings

Datasets Table 3 presents the datasets used in this experimental evaluation. The experiments cover real-world datasets with varying languages and training models, ranging in size from 1M to 10M vectors. The English datasets were trained using the SPLADE model, while the Chinese datasets were trained using the BGE-M3 model, which was developed internally by Ant Group. Notably, the Chinese datasets have significantly higher dimensionality compared to the English datasets, primarily due to the larger vocabulary size in Chinese. Table 3 also includes the average number of non-zero entries per vector ($avg \|x_i\|$) and the average number of vectors per inverted list ($avg l$), which can serve as references for selecting specific pruning parameters. Additionally, the experiments incorporate randomly generated datasets, in which both the number of non-zero entries and the corresponding values follow a random distribution. Table 3 further provides the *sparsity* of each dataset, which quantifies how sparse the data is. The *sparsity* of a dataset \mathcal{D} is calculated as: $sparsity = 1 - \frac{\sum_{x \in \mathcal{D}} \|x\|}{\|\mathcal{D}\| \cdot d}$, where $\|x\|$ denotes the number of non-zero entries in vector x (as defined in Definition 1), d is the maximum dimension, and $\|\mathcal{D}\|$ is the total number of vectors in \mathcal{D} .

We compare SINDI with five SOTA algorithms: SEISMIC, PYANNS, SOSIA, BMP, and HNSW. Below is a description of each algorithm:

- **SEISMIC** [2]: A sparse vector index based on inverted lists.
- **BMP** [3, 14]: A dynamic pruning strategy for learning sparse vector retrieval. It divides the original dataset into fine-grained blocks and generates a maximum value vector for each block to evaluate whether the block should be queried.

- **HNSW** [13]: A graph-based index designed for dense vector search. We adjusted the data format and distance computation to adapt it for sparse vectors.
- **PYANNS**: The open-source champion of the BigANN Benchmark 2023 Sparse Track. It is built on HNSW and incorporates quantization, query pruning, and rerank strategies.
- **SOSIA** [18]: A sparse vector index based on min-hash.

Parameter Settings We used the optimal parameters for each algorithm to ensure a fair evaluation. The parameter selection either follows the recommendations from the original authors or is determined through grid search.

Performance Metrics We evaluate the index construction time, index size, recall, and QPS for all baselines. Since approximate methods require a trade-off between query efficiency and accuracy, we use *throughput* to measure query efficiency, which is defined as the number of queries processed within a specific time interval. For a given query q , the result of Approximate Maximum Inner Product Search (AMPIS) is denoted as $R = \{\vec{x}_1, \vec{x}_2, \dots, \vec{x}_k\}$. Let $R^* = \{\vec{x}_1^*, \vec{x}_2^*, \dots, \vec{x}_k^*\}$ denote the exact top- k results obtained via Maximum Inner Product Search (MIPS). The recall is computed as follows: $Recall = \frac{|R \cap R^*|}{|R^*|}$. We specifically evaluate the recall metrics Recall@50 and Recall@100.

The experiments are conducted on a server with an Intel(R) Xeon(R) Platinum 8269CY CPU @ 2.50GHz and 512GB memory. We implement SINDI in C++, and compile it with g++ 10.2.1, -Ofast flag, and AVX-512 instructions enabled.

5.2 Overall Performance

5.2.1 Recall and QPS. Figure 8 analyzes the relationship between recall (Recall@50 and Recall@100) and the QPS performance of various algorithms on a single-threaded setup. For each algorithm, we report its best performance across all tested parameter configurations.

On both English and Chinese datasets, SINDI achieves the highest QPS under the same recall levels. When Recall@50 is 99%, on the SPLADE-1M dataset, the QPS of SINDI is 2.0× that of SEISMIC and 26.4× that of PYANNS; on the SPLADE-FULL dataset, the QPS of SINDI is 4.16× that of SEISMIC and 5.6× that of PYANNS. When Recall@100 is 98%, on the SPLADE-1M dataset, the QPS of SINDI is 1.9× that of SEISMIC and 3.2× that of PYANNS.

On the Chinese dataset encoded by the BGE-M3 model, SINDI also achieves the best performance. When Recall@50 is fixed at 97%, on the AntSparse-10M dataset, the QPS of SINDI is 2.5× that of SEISMIC. The RANDOM-5M dataset is generated uniformly at random, resulting in extremely sparse intersections of term IDs between data points. This sparsity causes the graph structures of

■ SINDI
 ◆ SEISMIC
 ◆ PYANNS
 ★ BMP
 ▲ SOSIA
 ● HNSW

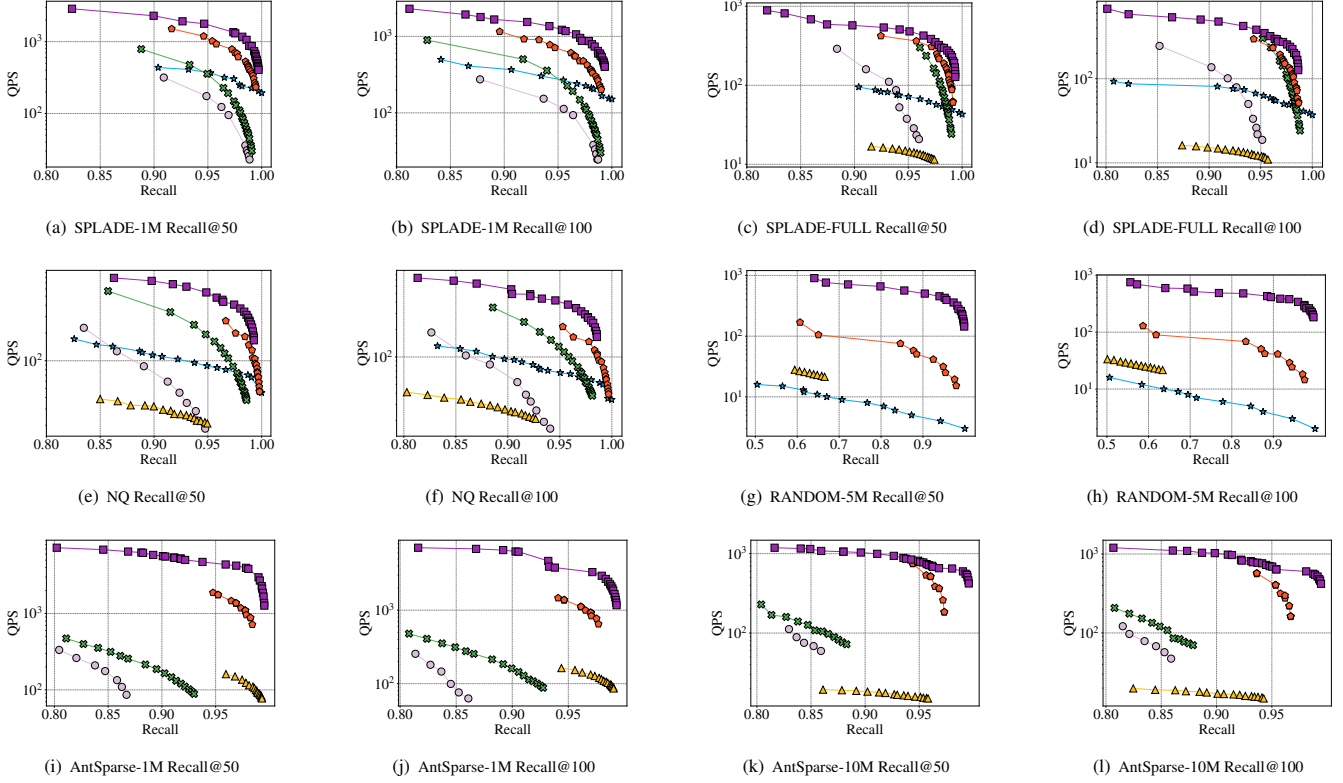


Figure 8: Overall Performance.

PYANNS and HNSW to become disconnected, leading to poor recall performance. The effectiveness of SEISMIC’s clustering is also sensitive to data distribution, causing noticeable performance degradation. In contrast, SINDI remains unaffected by data distribution and continues to achieve the best overall performance.

These results demonstrate that SINDI consistently achieves SOTA performance across datasets of various languages, models, and distributions.

5.2.2 Index Size and Construction Time. Figure 9 summarizes the index size and construction time for SINDI, SEISMIC, and PYANNS across three datasets. SINDI demonstrates the lowest construction cost across all datasets.

SEISMIC, which requires storing summary vectors for each block, results in the largest index size. On the NQ dataset, its size is 3× that of SINDI. On the other hand, PYANNS’ graph index construction involves a large number of distance computations to find neighbors, leading to extremely high construction time. For example, on the SPLADE-FULL dataset, PYANNS’ construction time is 71× that of SINDI. In contrast, SINDI’s index construction primarily involves sorting non-zero entries for pruning, which keeps the overall cost low and enables rapid index building.

5.3 Parameters

5.3.1 The Impact of α . This section explores how the document pruning parameter α affects SINDI’s performance. The parameter α determines the proportion of high-mass non-zero entries retained. For the MsMarco and NQ datasets, α is tested from 0.4 to 0.8, with a step size of 0.1. For the AntSparse dataset, α ranges from 0.7 to 1, with a step size of 0.05. Figure 10 presents the changes in recall and QPS as α increases under fixed β and γ . On the MsMarco dataset, recall improves and QPS decreases as α grows, but both changes slow down when α becomes larger. On the AntSparse dataset, recall also improves slowly, but QPS drops more rapidly. When α is small, increasing it retains more high-scoring non-zero entries, which boosts recall significantly. As α becomes larger, the additional retained entries have less impact, making recall improvements slower. For the AntSparse dataset, the scores of non-zero entries have smaller variance and are closer to zero compared to English datasets. This causes more non-zero entries to be retained as α increases, leading to a faster decrease in QPS compared to the MsMarco dataset.

5.3.2 The Impact of sparsity. We analyze the performance of SINDI under varying dataset *sparsity* levels. *sparsity* measures the proportion of non-zero entries in a dataset. For a fixed number of non-zero entries, larger dimensions result in higher *sparsity*. To investigate this, we generated five random datasets, each with 1M

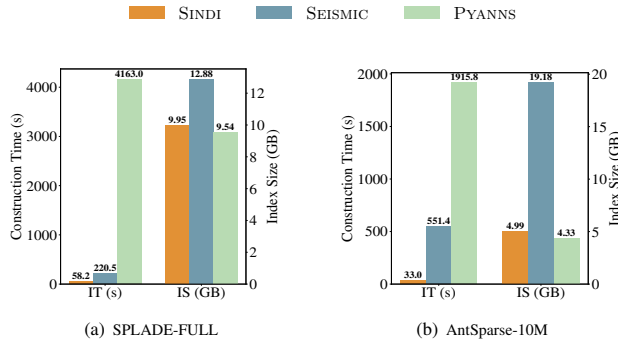


Figure 9: Index Size and Construction Time for Different Datasets and Algorithms.

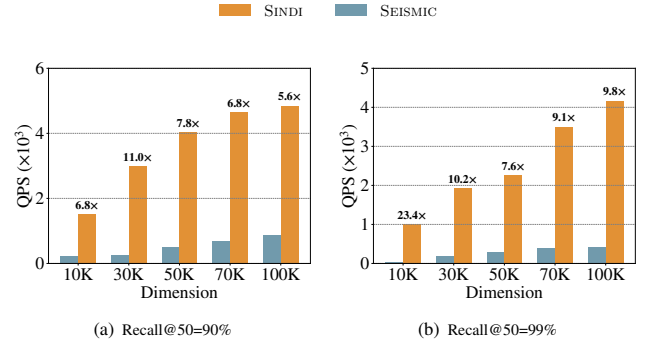


Figure 11: QPS of SINDI and SEISMIC on RANDOM-1M Dataset with different sparsity

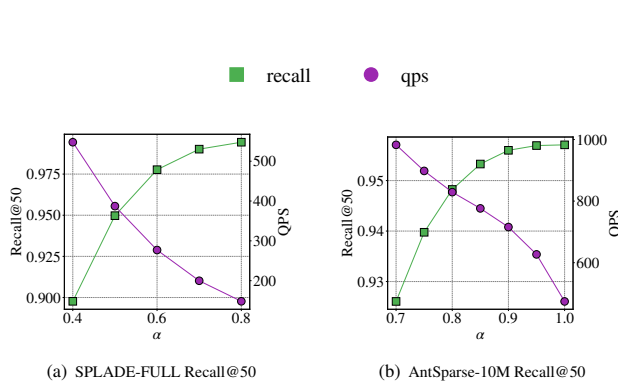


Figure 10: The Impact of α .

vectors and an average of 120 non-zero entries per vector. The dataset dimensions were set to [10,000; 30,000; 50,000; 70,000; 100,000], increasing *sparsity* progressively. Figure 11 compares the performance of SINDI and SEISMIC across these datasets on Recall@50 = 90% and Recall@50 = 99%.

The results show that as *sparsity* increases, both SINDI and SEISMIC achieve higher QPS at the same recall levels. This is because higher *sparsity* allows the IVF structure to partition data more effectively. As *sparsity* increases, each term list contains fewer vectors, which reduces the number of vector candidates that need to be searched during a query. Consequently, the number of inner product computations decreases, leading to improved QPS. Crucially, since all nearest neighbors are still captured within the lists, recall is not affected. In contrast, graph-based indexes face challenges with higher *sparsity*. Sparse high-dimensional data leads to weaker connectivity between nodes in the proximity graph, resulting in degraded search performance. Thus, IVF provide a natural advantage for sparse datasets compared with graph structure.

SINDI consistently outperforms SEISMIC by maintaining approximately 10 \times higher QPS across all *sparsity* levels. This demonstrates SINDI’s efficiency and scalability on sparse datasets. Additionally, SINDI is particularly suitable for languages like Chinese, where larger vocabularies result in high-dimensional and sparse datasets. Its ability to adapt to different *sparsity* levels and data distributions

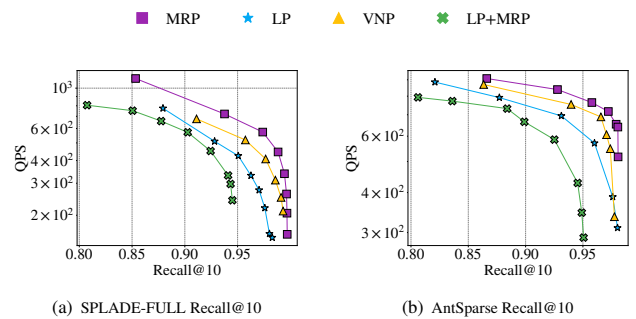


Figure 12: Recall@10 vs QPS on MsMarco and AntSparse of Mass Ratio Pruning, List Pruning and Vector Number Pruning.

highlights its robustness and wide applicability in real-world scenarios.

5.4 Ablation

5.4.1 The Impact of Pruning Method. Figure 12 illustrates the performance of different pruning strategies on the SPLADE-FULL and AntSparse datasets. The experiments evaluate all pruning strategies under the same β and γ settings, while varying α to measure Recall and QPS. The results demonstrate that *Mass Ratio Pruning* achieves the best performance, followed by *Vector Number Pruning* and *List Pruning*, with the lowest performance observed when combining *List Pruning* and *Mass Ratio Pruning*.

This is because *Mass Ratio Pruning* effectively preserves the non-zero entries that contribute the most to inner product computation, resulting in more true nearest neighbors being retained during the partial inner product stage. In contrast, *List Pruning* restricts the size of posting lists for each dimension, which creates two problems: some lists contain too few documents, retaining small-value entries, while others have too many documents, removing large-value entries. As a result, *List Pruning* is unsuitable for SINDI. In comparison, SEISMIC employs *List Pruning* since it computes the full inner product for all vectors within the lists, thereby avoiding significant losses in accuracy. However, when both *List Pruning* and *Mass Ratio Pruning* are applied simultaneously, more non-zero entries are discarded, leading to further decreases in recall.

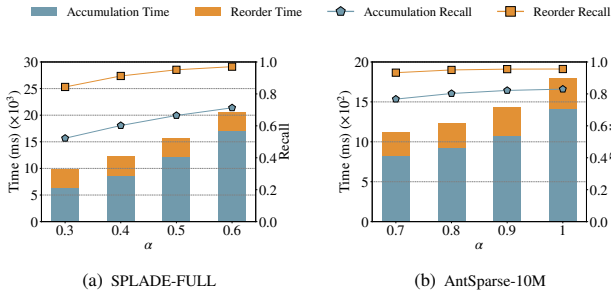


Figure 13: Reorder vs. Non-Reorder on SPLADE-FULL and AntSparse-10M Datasets: Time Cost and Recall@50 with Varying α .

5.4.2 The Impact of Reorder. To investigate the impact of the reordering strategy on the performance of SINDI, we compared the differences between using and not using reordering. Experiments were conducted on the SPLADE-FULL and AntSparse datasets. We set the query cut ratio β to 0.2 and reordering number γ top 500. The non-reordering strategy did not require storing dataset.

The results are shown in Figure 13. We evaluated the query time and Recall@50 for both strategies under various α . For the reordering strategy, the query time includes accumulation time and reordering time, while the non-reordering strategy only includes accumulation time. Since the parameter γ is fixed, the reorder time remains relatively constant. However, as α increases, the accumulation time grows accordingly. Although reorder time accounts for only a small portion of the overall query time, it significantly improves recall. For example, on the SPLADE-FULL dataset, when $\alpha = 0.6$, the accumulation time is 17099 ms, and the reorder time is 3553 ms. Despite this, the recall improves substantially from 0.71 to 0.97. This demonstrates the substantial efficiency improvement achieved by the reordering strategy.

The reordering strategy demonstrates its effectiveness for two reasons. First, it focuses on computing only a small subset of non-zero entries that contribute the most to the inner product, significantly reducing computations. Second, the partial inner product derived from high-mass entries can largely preserve the true ranking order of the inner product. This ensures that a small subset of candidate vectors is sufficient to include the true nearest neighbors, improving both efficiency and accuracy.

5.5 Scalability

To further evaluate the scalability of the SINDI algorithm, we conducted a multi-threaded performance test on two large-scale datasets: SPLADE-FULL and AntSparse-10M. We measured QPS at different recall targets (Recall@50 \in {0.91, 0.95, 0.999}) while varying the number of CPU cores from 2 to 10, as shown in Figure 14. On AntSparse-10M at Recall@50 = 0.90, using 2 CPU cores yields 1979.49 QPS (approximately 989.75 QPS per core), while using 10 cores achieves 8374.01 QPS (approximately 837.40 QPS per core). The per-core efficiency remains high, dropping by less than 16% when scaling from 2 to 10 cores. Similar scaling behavior is observed for SPLADE-FULL, confirming that SINDI effectively utilizes available CPU cores with minimal parallelization overhead.

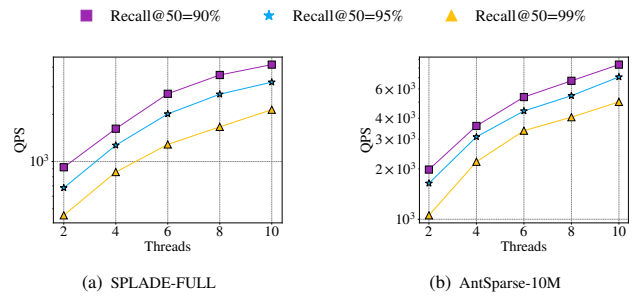


Figure 14: Multi-threaded scalability of SINDI (QPS) at different Recall@50 targets on SPLADE-FULL and AntSparse-10M datasets.

These results demonstrate that SINDI maintains high multi-core efficiency across datasets and accuracy levels, making it suitable for deployment in scenarios requiring both high recall and high throughput.

6 RELATED WORK

Existing methods for MIPS on sparse vectors adopt diverse index structures, including inverted index-, graph-, and hash-based designs. Inverted index-based methods, such as SEISMIC [2], build postings for each dimension and prune low-value entries to reduce the candidate set. They cluster postings into blocks to skip irrelevant candidates. However, as each vector appears in multiple postings, value retrieval still requires random access to scattered data.

Graph-based methods, such as HNSW-based PYANNS [13], organize vectors as nodes in a proximity graph. At query time, greedy graph traversal identifies neighbors, but vector sparsity leads to weak connectivity and frequent random memory accesses.

Hash-based methods, like SOSIA [18], transform sparse vectors into sets (via SOS) and use min-hash to estimate Jaccard similarity. Multiple hash functions improve accuracy but scatter vector storage across buckets, limiting locality and making direct computation in postings impractical.

BMP [3, 14] also stores non-zero values in postings and prunes with block-level maximum value vectors. While this avoids ID lookups, its fine-grained partitioning leads to excessive block evaluations, degrading efficiency. Our method retains value-stored postings without requiring costly block-level filtering.

7 CONCLUSION

In this work, we propose SINDI, an inverted index for sparse vectors that eliminates redundant distance computations. By storing term weights directly in the postings, SINDI removes both the ID lookup and random memory access overhead in distance computation, and leverages SIMD to fully exploit CPU parallelism. It further introduces *Mass Ratio Pruning* that preserves maximum inner-product accuracy while enabling scalable approximate search on large datasets. Experiments on multilingual, multi-scale real-world datasets demonstrate that SINDI achieves state-of-the-art performance.

REFERENCES

- [1] Dimitri Bertsekas and Robert Gallager. *Data networks*. Athena Scientific, 2021.
- [2] Sebastian Bruch, Franco Maria Nardini, Cosimo Rulli, and Rossano Venturini. Efficient inverted indexes for approximate retrieval over learned sparse representations. In *Proceedings of the 47th International ACM SIGIR Conference on Research and Development in Information Retrieval*, pages 152–162, 2024.
- [3] Parker Carlson, Wentai Xie, Shanxiu He, and Tao Yang. Dynamic superblock pruning for fast learned sparse retrieval. In *Proceedings of the 48th International ACM SIGIR Conference on Research and Development in Information Retrieval*, SIGIR '25, page 3004–3009, New York, NY, USA, 2025. Association for Computing Machinery.
- [4] Thibault Formal, Carlos Lassance, Benjamin Piwowarski, and Stéphane Clinchant. Splade v2: Sparse lexical and expansion model for information retrieval. *arXiv preprint arXiv:2109.10086*, 2021.
- [5] Thibault Formal, Carlos Lassance, Benjamin Piwowarski, and Stéphane Clinchant. From distillation to hard negative sampling: Making sparse neural ir models more effective. In *Proceedings of the 45th International ACM SIGIR Conference on Research and Development in Information Retrieval*, SIGIR '22, page 2353–2359, New York, NY, USA, 2022. Association for Computing Machinery.
- [6] Thibault Formal, Benjamin Piwowarski, and Stéphane Clinchant. Splade: Sparse lexical and expansion model for first stage ranking. In *Proceedings of the 44th International ACM SIGIR Conference on Research and Development in Information Retrieval*, SIGIR '21, page 2288–2292, New York, NY, USA, 2021. Association for Computing Machinery.
- [7] Yunfan Gao, Yun Xiong, Xinyu Gao, Kangxiang Jia, Jinliu Pan, Yuxi Bi, Yixin Dai, Jiawei Sun, Haofen Wang, and Haofen Wang. Retrieval-augmented generation for large language models: A survey. *arXiv preprint arXiv:2312.10997*, 2(1), 2023.
- [8] John L Hennessy and David A Patterson. *Computer architecture: a quantitative approach*. Elsevier, 2011.
- [9] Piotr Indyk and Rajeev Motwani. Approximate nearest neighbors: towards removing the curse of dimensionality. In *Proceedings of the thirtieth annual ACM symposium on Theory of computing*, pages 604–613, 1998.
- [10] Omid Keivani, Kaushik Sinha, and Parikshit Ram. Improved maximum inner product search with better theoretical guarantee using randomized partition trees. *Mach. Learn.*, 107(6):1069–1094, June 2018.
- [11] Patrick Lewis, Ethan Perez, Aleksandra Piktus, Fabio Petroni, Vladimir Karpukhin, Naman Goyal, Heinrich Küttler, Mike Lewis, Wen-tau Yih, Tim Rocktäschel, et al. Retrieval-augmented generation for knowledge-intensive nlp tasks. *Advances in neural information processing systems*, 33:9459–9474, 2020.
- [12] Guangyuan Ma, Yongliang Ma, Xuanrui Gou, Zhenpeng Su, Ming Zhou, and Songlin Hu. Lightretriever: A llm-based hybrid retrieval architecture with 1000x faster query inference. *arXiv preprint arXiv:2505.12260*, 2025.
- [13] Yu A. Malkov and D. A. Yashunin. Efficient and robust approximate nearest neighbor search using hierarchical navigable small world graphs. *IEEE Trans. Pattern Anal. Mach. Intell.*, 42(4):824–836, April 2020.
- [14] Antonio Mallia, Torsten Suel, and Nicola Tonello. Faster learned sparse retrieval with block-max pruning. In *Proceedings of the 47th International ACM SIGIR Conference on Research and Development in Information Retrieval*, SIGIR '24, page 2411–2415, New York, NY, USA, 2024. Association for Computing Machinery.
- [15] Ninh Pham. Simple yet efficient algorithms for maximum inner product search via extreme order statistics. In *Proceedings of the 27th ACM SIGKDD Conference on Knowledge Discovery & Data Mining*, KDD '21, page 1339–1347, New York, NY, USA, 2021. Association for Computing Machinery.
- [16] Yang Song, Yu Gu, Rui Zhang, and Ge Yu. Promips: Efficient high-dimensional c-approximate maximum inner product search with a lightweight index. In *2021 IEEE 37th International Conference on Data Engineering (ICDE)*, pages 1619–1630. IEEE, 2021.
- [17] Xiao Yan, Jinfeng Li, Xinyan Dai, Hongzhi Chen, and James Cheng. Norm-ranging lsh for maximum inner product search. *Advances in Neural Information Processing Systems*, 31, 2018.
- [18] Xi Zhao, Zhonghan Chen, Kai Huang, Ruiyuan Zhang, Bolong Zheng, and Xiaofang Zhou. Efficient approximate maximum inner product search over sparse vectors. In *2024 IEEE 40th International Conference on Data Engineering (ICDE)*, pages 3961–3974. IEEE, 2024.
- [19] Xi Zhao, Bolong Zheng, Xiaomeng Yi, Xiaofan Luan, Charles Xie, Xiaofang Zhou, and Christian S Jensen. Fargo: Fast maximum inner product search via global multi-probing. *Proceedings of the VLDB Endowment*, 16(5):1100–1112, 2023.